ARTICLE | OPEN ACCESS

Indian journal of
Engineering

To Cite:
Obaid ES, Salih EMS, Al-Shafaie SH. Effect of Microstructure on the Oxidation Behavior and Thermal Shock Resistance of Ti-17 Alloy. *Indian Journal of Engineering*, 2026, 23, e10ije1717
doi: https://doi.org/10.54905/disssi.v23i60.e10ije1717

Author Affiliation:
College of Materials Engineering, University of Babylon, Iraq

Contact list:
Eman S.Obaid emansolaiman66@yahoo.com
Ekbal Mohammed Saeed Salih mat.ekbal.moh@uobabylon.edu.iq
Saad Hameed Al-Shafaie mat.saad.hameed@uobabylon.edu.iq

Peer-Review History
Received: 09 November 2025
Reviewed & Revised: 16/December/2025 to 30/July/2026
Accepted: 12 August 2026
Published: 25 August 2026

Peer-Review Model
External peer-review was done through double-blind method.

Indian Journal of Engineering
pISSN 2319–7757; eISSN 2319–7765

© The Author(s) 2026. Open Access. This article is licensed under a Creative Commons Attribution License 4.0 (CC BY 4.0)., which permits use, sharing, adaptation, distribution and reproduction in any medium or format, as long as you give appropriate credit to the original author(s) and the source, provide a link to the Creative Commons license, and indicate if changes were made. To view a copy of this license, visit http://creativecommons.org/licenses/by/4.0/.

Effect of Microstructure on the Oxidation Behavior and Thermal Shock Resistance of Ti-17 Alloy

Eman S Obaid, Ekbal Mohammed Saeed Salih, Saad Hameed Al-Shafaie

ABSTRACT

The microstructure features of Ti-17 titanium alloy are very important to its mechanical properties and high-temperature life. In this work, the effect of compositional changes on the microstructure, hardness and oxidation resistance and thermal shock behavior of Ti-17 alloys was thoroughly studied. Seven compositions of Ti-17 alloy with various concentrations of Al, Mo, Cr and Zr were successfully produced by powder metallurgy by powder mixing, cold compaction and argon shielded sintering at 1500°C. The fabricated alloys were characterized by X-ray diffraction (XRD), optical microscopy, scanning electron microscopy (SEM) with energy-dispersive X-ray spectroscopy (EDX), Brinell hardness testing, high-temperature oxidation tests at 600, 700 and 800°C, and thermal shock tests at 600 and 700°C. The findings showed that changes in the amounts of the alloying elements had a considerable effect on the balance of the α/β phases and therefore on the mechanical and thermal characteristics. Alloy No. 4(82Ti-2Sn-2Zr-5Al-5Mo-4Cr) had the best overall performance of 402 HB, which was about 2.3% higher than the typical Ti-17 alloy (396 HB). The alloy also displayed the lowest oxidation weight increase at 800°C, suggesting better oxidation resistance owing to the creation of a stable and adherent protective oxide layer and simultaneously the strongest resilience to thermal shock under cyclic heating and cooling circumstances. The better performance was due to the optimal balance of α- and β-phase stabilizing elements, which resulted in a finer microstructure and improved oxide-scale stability. These results demonstrate that the controlled compositional optimization of Ti-17 alloys prepared by powder metallurgy is an effective strategy to enhance hardness, oxidation resistance and thermal shock resistance simultaneously, which makes the optimized alloy a promising candidate for high-temperature aerospace and advanced engineering applications.

Keywords: Ti-17, Oxidation, Thermal Shock, Microstructure.

1. INTRODUCTION

Titanium (Ti) and their alloys have a number of beneficial qualities, but the high initial cost has been one of the main difficulties of using them as structural materials (Ali et al., 2024). However titanium and its alloys are widely used in rocket engines (RE), gas turbine engines (GTE) (Jasim & Radhi, 2024) and aircraft

constructions. The expense can be a limiting factor, particularly for use in airframes where competing alloys are usually many times cheaper. However, titanium is priced comparably or even lower than other materials for GTE and RE applications, so cost is less of a concern. The critical need of weight reduction in spacecraft design (Besisa & Yajima, 2024; Jawed et al., 2022) also further separates cost concerns.

Titanium and titanium alloys are highly sensitive to impurities, especially to ambient oxygen and nitrogen. Even fractions of a percent or less of these elements can profoundly alter the properties of titanium by forming interstitial solid solutions or metallic phases in the alloy. Such sensitivity is reflected in a wide gamut of grades of first semi-finished products, i.e. porous titanium sponges (Marin & Lanzutti, 2023). Titanium is used in many applications. Its properties can be altered by varying the composition of alloying elements. This shows the versatility of titanium. It changes its allotropic form. At room temperature, titanium is in the hexagonal close packed (HCP) alpha phase. On heating to about 883 °C it changes to the beta phase with a body-centered cubic (BCC) structure. These different crystal structures are sometimes referred to as "phases." Transformation Temperature: The temperature at which titanium changes from the alpha phase to the beta phase. Fig. 1 shows the crystal structure of pure titanium (Quinn et al., 2020).

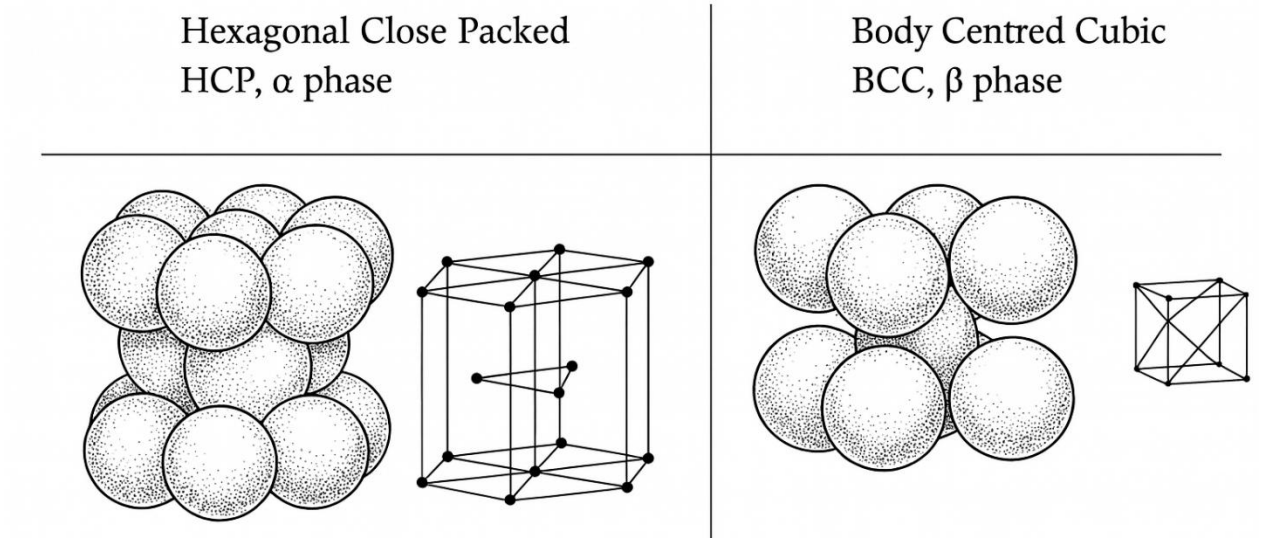


Figure 1. The two main crystal structures of Ti.

Luo et al., (2014) studied the microstructural evolution of Ti-17 alloy during the isothermal compression test. Wang et al., (2011) investigated the dynamics of grain development in the _ phase of Ti-17 alloys Ti-17 alloy dynamics in the β-phase. Teixeira et al., (2007) and Tarín et al., (2006) studied the microstructural evolution and transformation kinetics of Ti-17 titanium alloy under continuous cooling, and studied the ultimate tensile strength, yield strength and elongation of Ti-17 alloy. Xu et al., (2016) have reported the linear correlation between tensile properties and globularization fraction in their work on the effect of globularization behavior of lamellar alpha on tensile properties of Ti-17 alloy. Moshier et al., (2001) investigated the effect of load history on the fatigue crack initiation threshold of Ti-17 alloy. The microstructure containing long and thick needle-like α platelets exhibited higher fracture toughness and strength than that containing short rod-like α platelets. Shi et al., (2016) Study of the Influence of Lamellar Features on the Fracture Toughness of Ti-17 Titanium Alloy. Titanium alloys are categorized into several types depending on their microstructure and alloying elements (Elshaer & Ibrahim, 2022).

- **Alpha Alloys** are mainly based on the alpha phase. They have good corrosion resistance and are easily weldable. They have good high-temperature properties, but are often weaker than other varieties. E.g. Ti-5Al-2.5Sn (titanium alloy with 5% aluminum and 2.5% tin).
- **Beta Alloys** Dominated by the beta phase, these alloys can be heat treated to achieve high strength and improved mechanical properties. However, their corrosion resistance is typically lower than that of alpha alloys-example: Ti-3Al-8V-6Cr-4Zr-4Mo (known as Beta C alloy) (Court et al., 2001).

- **Alpha-Beta** Alloys Consisting of a mixture of alpha and beta phases, these alloys offer a balanced combination of strength, corrosion resistance, and weldability, making them the most commonly used titanium alloys-example: Ti-6Al-4V (containing 6% aluminum and 4% vanadium), widely used in aerospace and medical fields, Ti 17(Ti-5Al-2Sn-4Cr-2Zr-4Mo) (Jasim and Radhi, 2024; Narayan, 2012).

Ti-17 (Ti-5Al-2Sn-2Zr-4Cr-4Mo) high-performance titanium alloy Ti 17 is renowned for its exceptional strength, corrosion resistance, and thermal stability. It is frequently utilized in applications needing dependable performance at somewhat higher temperatures and is a member of the near-alpha class of titanium alloys. Its well-balanced composition allows it to keep the structural integrity under adverse conditions (Antunes et al., 2018; Valdez et al., 2012). Alpha stabilizers are Al and Sn which increase the strength of the alloy and the thermal stability at elevated temperatures (Abed et al., 2022; Radhi & Al-Khafaji, 2018). Zirconium (Zr) enhances mechanical properties and corrosion resistance. Microstructure control and improvement of toughness and strength are achieved by using beta stabilizers such as molybdenum (Mo) and chromium (Cr). Most Ti-17 has a microstructure consisting of a mixture of alpha phase grains with a small amount of beta phase along the grain boundaries. The microstructure of the alloy provides a unique combination of mechanical properties (Abd-Elaziem et al., 2024).

Titanium and its alloys are indispensable to a wide range of industries due to their unique combination of high strength, corrosion resistance and biocompatibility. They are used in the structure and engine parts of airplanes to reduce weight and improve fuel economy (Abd-Elaziem et al., 2024). Titanium is biocompatible with the human body and mechanically robust so it is ideal for biomedical applications such as dental screws and joint replacements. Titanium is used in the marine industry because it does not corrode in sea water. It is therefore useful in the production of parts of ships and off-shore constructions. Titanium is safe and durable and is used in the chemical processing industry to manufacture equipment that will come in contact with hostile chemicals such as heat exchangers and reactors. More significantly, it promotes the production of lightweight, high-performance automotive components, leading to increased engine efficiency and decreased fuel consumption (Tao et al., 2024).

Although there are several publications on the mechanical behavior and phase transition features of Ti-17 alloy, some crucial information gaps still exist. So far, research have mostly dealt with the microstructural development during thermomechanical processing. Still the effect of compositional alterations, regulated, on high-temperature oxidation and thermal shock resistance has been studied less. Furthermore, most of the prior studies use normally produced wrought materials and there is very little information available on Ti-17 alloys made via powder metallurgy. In particular, the link between changed alloy chemistry, α/β phase balance, hardness, oxidation resistance and thermal shock performance has not been proven systematically. Therefore, an optimal Ti-17 mixture that may concurrently enhance these qualities has not been explicitly found yet.

The originality of the current study resides in the systematic compositional optimization of powder metallurgy Ti-17 alloys by controlled change of the Al, Mo and Cr concentrations, while retaining the Ti-17 alloy system. As opposed to earlier investigations which have been mostly concerned with the deformation behaviour or conventional mechanical characteristics, the current study makes a direct link between alloy chemistry, microstructural development, hardness, oxidation resistance and thermal shock resistance. Seven Ti-17 alloy compositions were produced by powder metallurgy and evaluated in detail by XRD, optical microscopy, SEM/EDX, hardness, oxidation studies at 600–800 °C and thermal shock testing. The investigation has identified an optimum composition, Ti-82Al-5Sn-2Zr-2Mo-5Cr-4 (Alloy No. 4; nominally 82Ti-2Sn-2Zr-5Al-5Mo-4Cr), which shows the maximum hardness (402 HB), better oxidation resistance at 800°C and improved thermal shock resistance. The results suggest a feasible compositional design approach to improve the high-temperature performance of Ti-17 alloys for advanced aerospace applications.

2. EXPERIMENTAL WORK

Ti-17 alloys were fabricated using commercially pure elemental powders of titanium (Ti), aluminum (Al), tin (Sn), zirconium (Zr), molybdenum (Mo), and chromium (Cr) with a purity of ≥99.5 wt. % and an average particle size of 55 μm as the starting ingredients. The chemical composition of the reference Ti-17 alloy obtained by elemental analysis is shown in Table 1. The nominal compositions of the seven experimental versions of alloys studied in this work are described in Table 2. The powders were weighed correctly according to the prescribed compositions and homogenized in a planetary ball mill at 200 rpm for 4 h with a ball to powder weight ratio of 5:1 to achieve uniform elemental distribution before consolidation. The mixed powders were then compacted by uniaxial cold pressing at 650 MPa to get cylindrical green compacts of 15 mm in diameter and 10 mm in height. The green samples were sintered in a high-temperature tube furnace under continuous flow of high-purity argon gas (99.999%) at a flow rate of around 1 L min−1 to reduce

oxidation throughout the thermal procedure. The furnace was heated to 1500°C at a regulated heating rate of 10°C min-1 and was held at the peak temperature for 2 h to achieve complete diffusion and microstructural uniformity. It was then furnace cooled to room temperature at an average rate of around 5 °C min-1 in the same inert atmosphere.

X-ray diffraction (XRD) was used for phase identification and optical microscopy and scanning electron microscopy combined with energy dispersive X-ray spectroscopy (SEM/EDX) to study microstructural features and elemental distributions. The mechanical performance was tested by Brinell hardness test according to the ASTM E10 standards using a 10 mm diameter hardened steel ball indenter, an applied load of 3000 kg (29.42 kN) and dwell period of 15 s. Each specimen was indented five times at various points and average hardness value was recorded. The high-temperature oxidation behavior was tested at 600, 700 and 800°C in static laboratory air for the exposure times of 30 min to 3 h and the oxidation resistance was evaluated by the weight increase measurement using an analytical scale with an accuracy of ±0.1mg. Then, the thermal shock resistance was measured by repeatedly heating the specimens to 600 and 700 °C and quickly cooling them in ambient air. The surface morphology and weight change were analyzed to determine the thermal stability of the oxide layer. Three different specimens were evaluated for each experimental condition for reliability and reproducibility of the experimental data and all stated findings are the average values derived from the repeated measurements.

Table 1. chemical composition of Ti-17 alloy.

Element	Chemical composition [%]										
	Ti	Al	Sn	Zr	Cr	Mo	Fe	P	Ge	Ni	Cu
Ti-17	80.537	5.475	2.558	1.744	6.182	2.946	0.201	0.237	0.012	0.067	0.040

Table 2. Alloys used in this search

No	Ti	Sn	Zr	Al	Mo	Cr
1	83	2	2	6	4	4
2	82	2	2	6	4	4
3	84	2	2	4	4	4
4	82	2	2	5	5	4
5	84	2	2	5	3	4
6	82	2	2	5	4	5
7	84	2	2	5	4	3

3. RESULTS & DISCUSSIONS

X-Ray Diffraction Analysis

Figure 2 shows the X-ray diffraction (XRD) pattern of the as-prepared Ti-17 alloy. The diffraction profile suggests that the alloy is mostly made of α-Ti phase with hexagonal close-packed (HCP) crystal structure and a little amount of retained β-Ti phase with body-centered cubic (BCC) structure, which is characteristic of near-β titanium alloys. The principal diffraction peaks at around 2θ = 35.1°, 38.4°, 40.2°, 53.0°, 63.1°, 70.7° and 76.2° are assigned to the (100), (002), (101), (102), (110), (103) and (112) crystallographic planes of α-Ti, respectively, by comparing with the standard diffraction data (ICDD PDF No. 44-1294). In addition, faint diffraction peaks of β-phase are seen at around 2θ = 38.9°, 55.6° and 69.7°, which are ascribed to the (110), (200) and (211) planes of BCC β-Ti (ICDD PDF No. 44-1288). The weak intensity of the β-phase reflections shows that the microstructure is still mostly α-phase after sintering. But the presence of β-phase stabilizing elements, especially Mo and Cr, helps to retain a small amount of β-phase throughout cooling.

In contrast, α stabilizers like Al and Sn improve the stability of the HCP matrix, while Zr solid-solution enhances the stability without much change in the phase composition. The overall phase constituents are identical for the analyzed alloy compositions but differences in the relative amounts of α- and β-stabilizing elements are predicted to alter the α/β phase balance. More specifically, Alloy No. 4 (82Ti-2Sn-2Zr-5Al-5Mo-4Cr) is projected to have a finer $\alpha+\beta$ microstructure, as it has the greatest Mo amount of the studied alloys, although it is an optimal Al content. This precise distribution of phases leads to the higher hardness, oxidation resistance and thermal shock behaviour seen experimentally. No further diffraction peaks related to undesired secondary phases or intermetallic compounds were found, suggesting that the alloy was successfully homogenized throughout the powder metallurgy processing and sintering. In the current investigation, only a qualitative XRD analysis was conducted and quantitative phase fractions of the α and β-

phases were not identified. Future study using Rietveld refinement is advised to properly measure phase fractions and lattice characteristics, to get a more thorough knowledge of phase development in Ti-17 alloys.

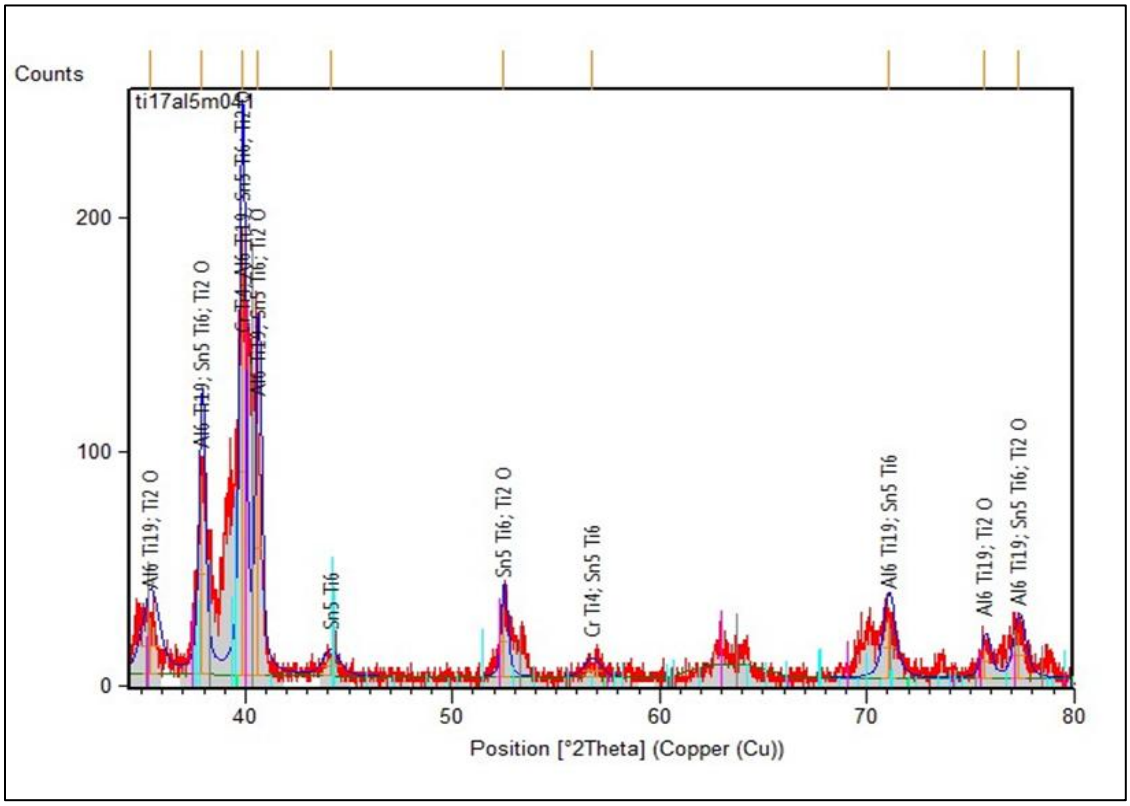


Figure 2. X-ray diffraction for Ti-17

Microstructure Observation of the Sintered Samples

Figure 3 Optical micrographs of the specimens of sintered Ti-17 alloy Effect of Alloy Composition on the Microstructural Development of the Seven Alloys Investigated The calculated aluminum equivalent (Aleq) for each alloy is listed in Table 3. It is a quantitative measure of the α-phase stabilizing effect due to the combined action of Al, Sn and Zr. The highest Aleq value (7.03) was observed for Alloy No. 2, which shows the maximum alpha-phase stability among the alloys studied, while the lowest Aleq (4.03) was determined for Alloy No. 5, indicating a relatively low tendency for the formation of the α-phase. In agreement with these estimated values, optical micrographs show that all the alloys display a distinctive dual-phase microstructure of near-β titanium alloys, consisting of a light-colored α-phase dispersed in a darker β-phase matrix. The relative proportion and shape of these phases are mainly controlled by the balance of α-stabilizing elements (Al and Sn) and β-stabilizing elements (Mo and Cr).

The increased aluminum content leads to better stability and volume percentage of the α phase. The higher molybdenum and chromium contents help in retaining the β-phase during cooling, thereby leading to a finer and more homogenous α+β microstructure. Alloy No. 4 (82Ti-2Sn-2Zr-5Al-5Mo-4Cr) has the most uniform and refined microstructure, due to the optimum balance between α- and β-stabilizing elements, while Alloy No. 2 has the greatest aluminum equivalent. This optimized microstructure with uniform distribution of tiny α lamellae in the β matrix efficiently prevents dislocation movement and is in agreement with the excellent hardness, oxidation and thermal shock resistances, which are described in the next sections. Alloys with lower contents of β stabilizers, in contrast, have coarser α-phase regions and a less homogenous phase distribution, which can have a negative impact on their mechanical and high-temperature performance. Some examples have a small amount of residual porosity, which arises from the powder metallurgy processing technique, although the comparatively low pore content suggests adequate densification during sintering. To allow for the quantitative interpretation of the microstructure, all optical micrographs in Fig. 3 should be provided with clearly visible scale bars and with increased picture quality. Furthermore, quantitative image analysis with software such as ImageJ is suggested in an effort to assess the average grain size and the α/β phase fraction, and therefore, to determine statistical correlations

between the summarized microstructural characteristics in Table 3 and the measured hardness, oxidation resistance and thermal shock behavior of the studied Ti-17 alloys (Gao et al., 2024).

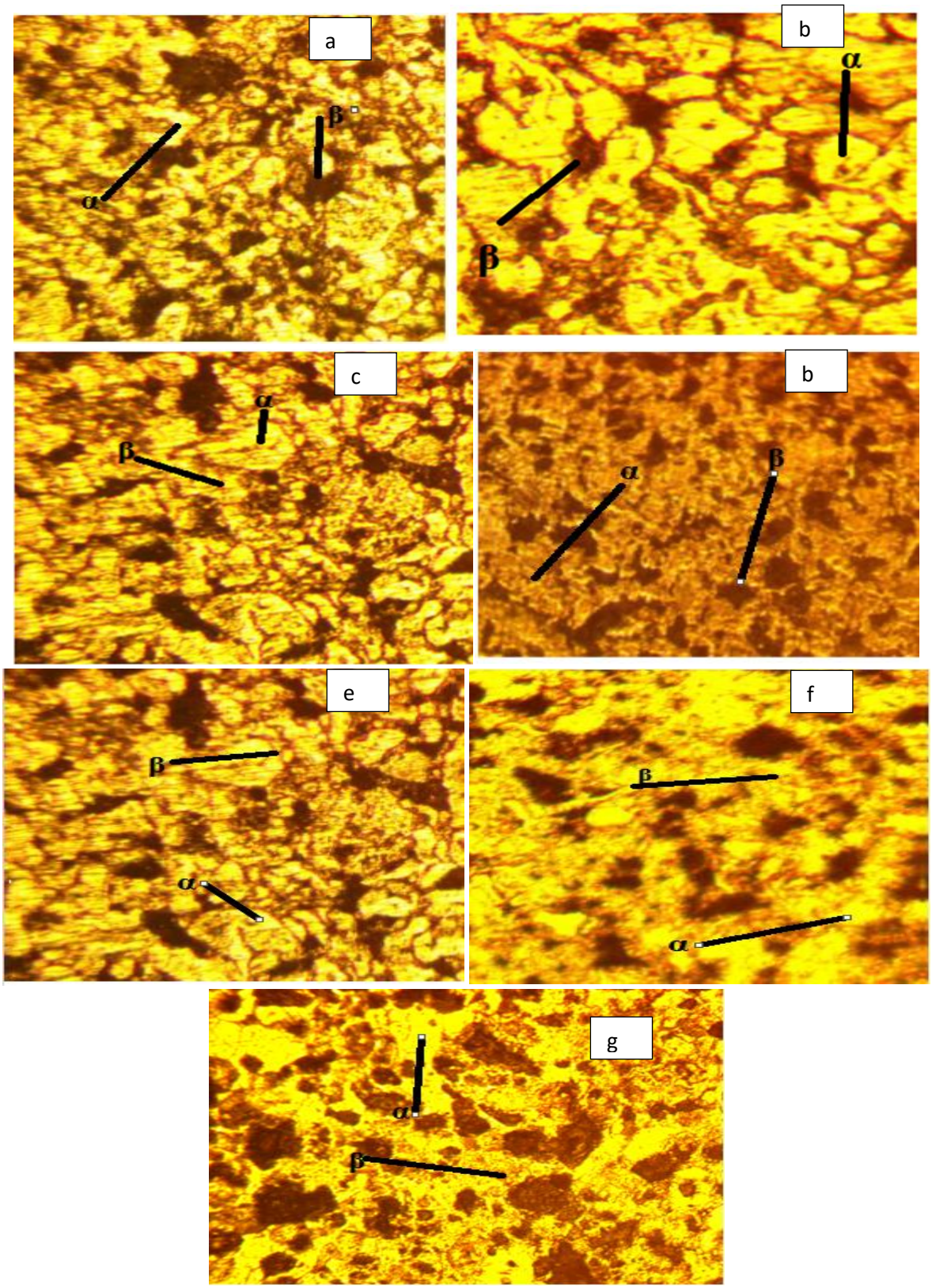


Figure 3. Microstructure of Ti-17: samples: a) 1; b) 2; c) 3; d) 4; e) 5; f) 6; g) 7

Table 3. Al equivalent.

Samples	Al equivalent
1(83Ti2Sn2Zr5Al4Mo4Cr)	6.03
2(82Ti2Sn2Zr6Al4Mo4Cr)	7.03
3(84Ti2Sn2Zr4Al4Mo4Cr)	5.03
4(82Ti2Sn2Zr5Al5Mo4Cr)	6.03
5(84Ti2Sn2Zr5Al3Mo4Cr)	4.03
6(82Ti2Sn2Zr5Al4Mo5Cr)	6.03
7(84Ti2Sn2Zr5Al4Mo3Cr)	6.03

SEM (Scanning Electrons Microscopies) and EDX (Energized Disperses X-ray Spectroscopies)

The scanning electron microscopy (SEM) micrographs and the corresponding energy-dispersive X-ray spectroscopy (EDX) spectra of the seven Ti-17 alloy compositions are shown in Figure 4. The nominal chemical compositions of the investigated alloys are summarized in Table 2, and the calculated aluminum equivalent values are listed in Table 3. The SEM data agree with the dual-phase microstructure seen via the optical microscope which is a continuous α-phase matrix with scattered patches of β-phase. The shape and distribution of these phases will be dependent upon the relative concentrations of the α-stabilizing elements (Al and Sn) and the β-stabilizing elements (Mo and Cr). Higher content of Mo and Cr alloys have finer and more uniform distribution of β-phase. Higher content of Al alloys has larger fraction of α phase, which is in accordance with the rising Al equivalent values shown in Table 3. Among the examined compositions, the most homogenous microstructure with refined α+β phase distribution and relatively low density of microstructural defects is seen for the Alloy No. 4 (82Ti–2Sn–2Zr–5Al–5Mo–4Cr), which testifies to the effective diffusion and homogeneity during sintering process.

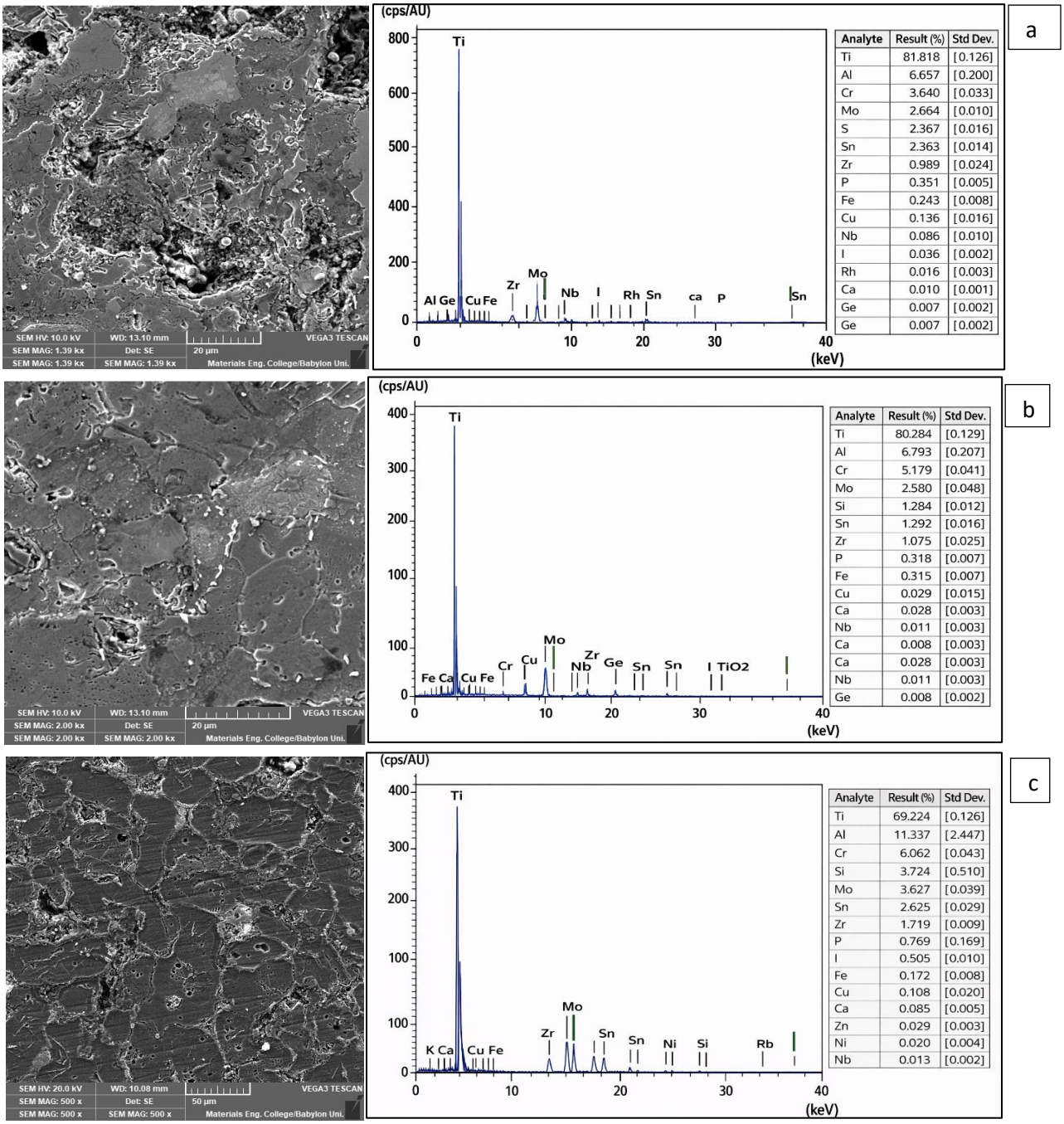
Conversely, alloys with low concentrations of β-phase stabilizers have coarser α-phase regions and more microstructural variability, which may adversely affect their mechanical and high-temperature performance. The SEM pictures show indicate the existence of isolated holes dispersed throughout the microstructure, which are ascribed to the insufficient densification in powder metallurgy process. The observed porosity is very modest but the holes may act as preferential diffusion pathways for oxygen during high-temperature exposure and as areas of stress concentration during thermal cycling triggering oxide-scale cracking and localized oxidation. This agrees with the oxidation findings of the alloys shown in Tables 5–7 where the alloys with finer and more uniform microstructure notably the Alloy No. 4 showed the lowest oxidation weight increase at 600, 700 and 800°C indicating greater oxidation resistance. The corresponding EDX spectra of all the examined alloys are shown in Figure 4 and are in agreement with the presence of Ti, Al, Sn, Zr, Mo and Cr without any sign of undesirable impurity phases, confirming the efficient alloy preparation and chemical homogeneity. Moreover, the distribution of the measured elements is in excellent agreement with the nominal alloy compositions presented in Table 2, indicating that the desired compositional changes were really obtained during powder mixing and sintering. The increased oxidation resistance of Alloy No. 4 is ascribed to the appropriate mix of Al, Mo and Cr, which favors the production of a thick and adherent protective oxide layer, and the refined microstructure of a+β, which hinders the diffusion of oxygen into the alloy matrix.

However, in the current inquiry, point EDX analysis was used to confirm the elemental composition. In future investigations, elemental distribution maps (EDS mapping) should be used to observe the spatial distribution of Ti, Al, Sn, Zr, Mo and Cr throughout the microstructure. Moreover, it is also suggested to use quantitative image analysis using software such as ImageJ for the quantification of the total porosity percentage and pore-size distribution to establish quantitative relationships between porosity, oxidation kinetics and the mechanical performance of powder metallurgy Ti-17 alloys.

Hardness Test

Table 4 and Figure 5 show the Brinell hardness data for the reference Ti-17 alloy and the 7 alloy compositions produced. The results indicate that the change of the concentrations of the a- and b-stabilizing elements had a significant effect on the hardness of the investigated alloys, affecting the phase balance and the microstructure refinement. The hardness of the standard Ti-17 alloy was 396 HB, and the hardness of the fabricated alloy was in the range of 385 to 402 HB. The highest hardness 402 HB was obtained for the alloy No. 4 (82Ti-2Sn-2Zr-5Al-5Mo-4Cr) among all the investigated compositions, which is higher by approximately 1.52% than the reference Ti-17 alloy. The improvement is due to the optimized balance between α- and β-stabilizing elements, especially the increased

molybdenum content, which promoted the stabilization of β-phase, solid-solution strengthening, and the formation of a finer $\alpha + \beta$ microstructure, as evidenced by the optical microscopy and SEM observations in Figures 3 and 4.



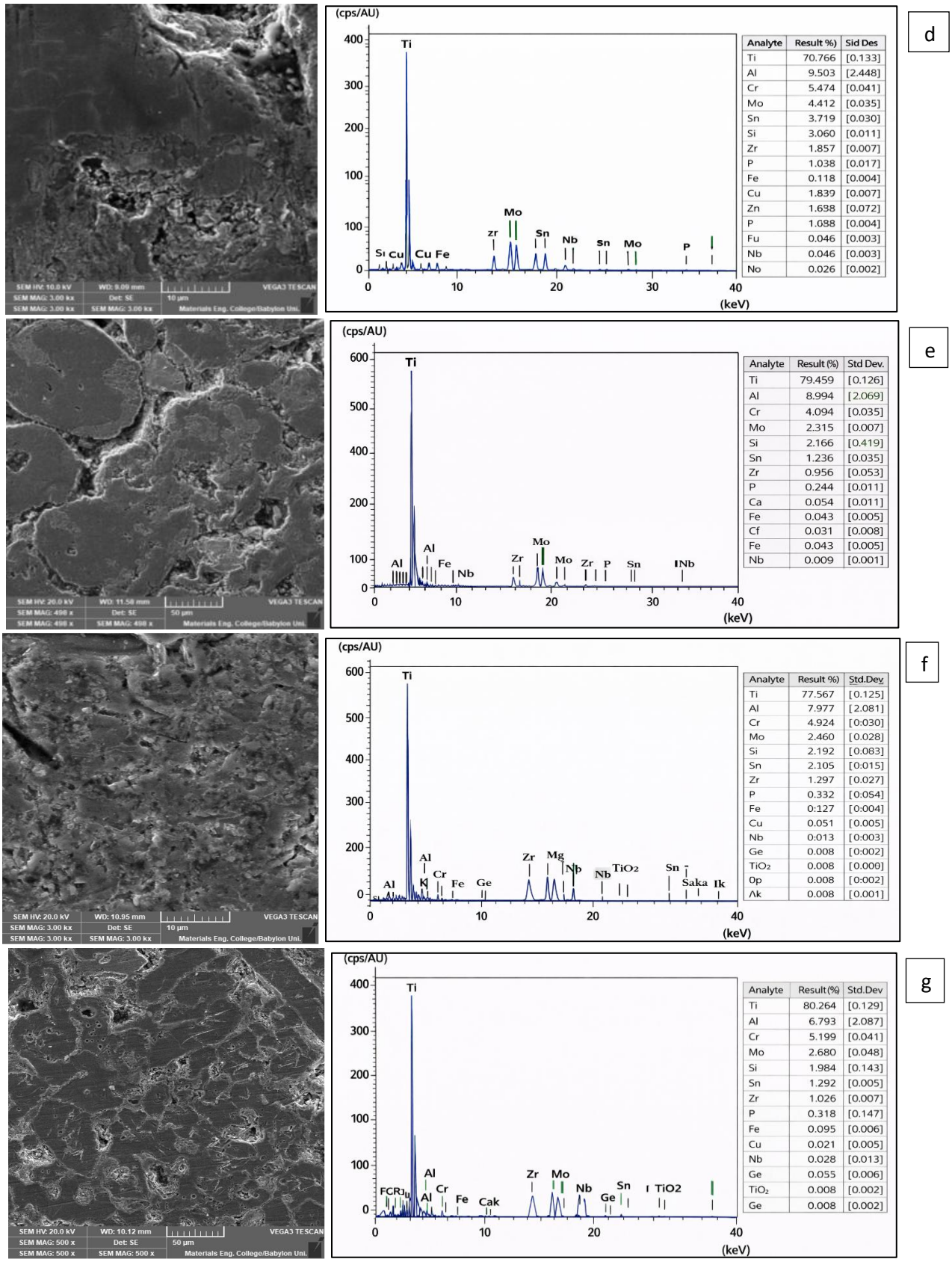


Figure 4. SEM and EDX for Samples: a) 1; b) 2; c) 3; d) 4; e) 5; f) 6; g) 7.

In contrast, the hardness of Alloy No. 2 increased slightly to 397 HB, which was an improvement of around 0.25% whilst Alloy No. 1 showed 393 HB, a small decrease of 0.76% compared to the reference alloy. Alloys No. 3, 5, 6, and 7 have lower hardness values, with decreases of around 1.26%, 2.78%, 1.52%, and 2.02%, respectively. The lowest hardness was found for Alloy No. 5 (385 HB), showing that the reduction in the quantity of molybdenum decreased the stability of β-phase and impaired the strengthening effect given by solid solution hardening. Likewise, lower hardness of Alloy No. 7 implies that reduction in chromium concentration has a negative effect on microstructural refinement and resistance to plastic deformation.

Table 4. The hardness value of the selected samples alloys.

Material	Composition (wt.%)	Hardness (HB)	Improvement rate (%)
Reference Ti-17	83Ti–2Sn–2Zr–5Al–4Mo–4Cr	396	0.00
Alloy 1	83Ti–2Sn–2Zr–6Al–4Mo–4Cr	393	−0.76
Alloy 2	82Ti–2Sn–2Zr–6Al–4Mo–4Cr	397	+0.25
Alloy 3	84Ti–2Sn–2Zr–4Al–4Mo–4Cr	391	−1.26
Alloy 4	82Ti–2Sn–2Zr–5Al–5Mo–4Cr	402	**+1.52**
Alloy 5	84Ti–2Sn–2Zr–5Al–3Mo–4Cr	385	−2.78
Alloy 6	82Ti–2Sn–2Zr–5Al–4Mo–5Cr	390	−1.52
Alloy 7	84Ti–2Sn–2Zr–5Al–4Mo–3Cr	388	−2.02

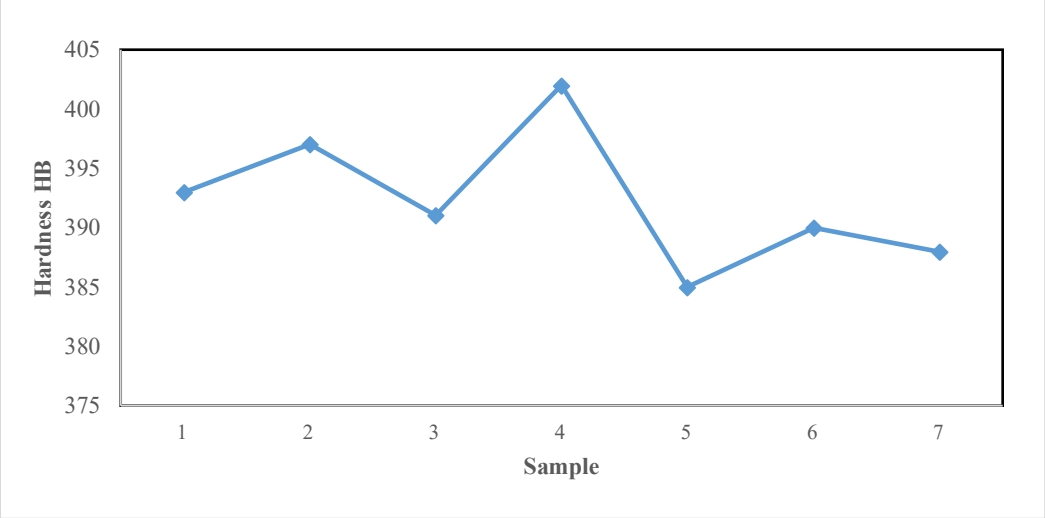


Figure 5. Hardness for all samples.

Oxidation Inside the Furnace

The high-temperature oxidation behavior of the produced Ti-17 alloys at 600, 700, and 800°C was studied and the respective weight increase findings are shown in Tables 5–7 and Figures 6–8. Oxidation resistance was shown to depend significantly on the exposure temperature and the alloy composition. For all studied alloys the oxidation weight gain was found to rise with increasing temperature and exposure duration showing step-wise oxide-scale development during thermal exposure. At 600°C all the alloys showed a minimal weight increase which indicated the production of a thin, continuous and adhesive oxide coating which successfully restricted the migration of additional oxygen into the substrate. The oxidation kinetics were accelerated at 700C due to the higher ionic transport through the oxide layer and all compositions showed greater weight gain. The greatest oxidation rates were found at 800°C where the enhanced diffusion rate allowed fast oxide formation and resulted in greater thermal stresses in the oxide scale, diminishing its protective efficiency. However, the oxidation resistance was found to vary greatly for the alloys studied. Alloy No. 4 (82Ti–2Sn–2Zr–5Al–5Mo–4Cr) showed the lowest oxidation weight increase at all temperatures studied and the maximum oxidation resistance, as described in Tables 5–7 and Figure 9.

The improved behavior is attributable to the adjusted balance of Al, Mo and Cr, which favors the production of dense and adherent TiO2-based oxide layer enriched by protective Al2O3 and Cr-containing oxides. The addition of molybdenum also helps to reduce

oxygen migration through the β-phase and increases the microstructural stability over long term exposure to high-temperatures. These findings are in agreement with the enhanced α+β microstructure seen by optical microscopy and SEM examinations (Figure 3 and 4), where Alloy No. 4 showed more homogeneous phase distribution and lowest apparent porosity. Thus, the lower interconnected porosity gave less rapid diffusion pathways for oxygen, delaying the growth of the oxide scale and improving the oxidation resistance. The oxidation behavior of titanium alloys is normally dominated by diffusion-controlled kinetics and typically follows a parabolic oxidation law. The oxidation rate steadily reduces as the protective oxide layer thickness increases. In the current work, the oxidation resistance was assessed using weight-gain measures, however the parabolic oxidation rate constants were not calculated and no quantitative kinetic modeling was undertaken. Likewise, characterization by XRD following oxidation, cross-sectional SEM observations and oxide-scale thickness measurements were beyond the scope of the current work (Niinomi, 2003).

Table 5. oxidation at 600°C

sample	ΔW After 30 min	ΔW After 1 h	ΔW After 1.30 h	ΔW After 2 h	ΔW After 2.30 h	ΔW After 3 h
1(83Ti2Sn2Zr5Al4Mo4Cr)	0.0392	0.1083	0.2310	0.2861	0.3421	0.3421
2(82Ti2Sn2Zr6Al4Mo4Cr)	0.0134	0.1130	0.1106	0.1354	0.2086	0.2086
3(84Ti2Sn2Zr4Al4Mo4Cr)	0.0271	0.1065	0.1941	0.2035	0.2117	0.2116
4(82Ti2Sn2Zr5Al5Mo4Cr)	0.0311	0.1021	0.1083	0.1161	0.1845	0.1844
5(84Ti2Sn2Zr5Al3Mo4Cr)	0.0221	0.0368	0.1270	0.1289	0.2045	0.2045
6(82Ti2Sn2Zr5Al4Mo5Cr)	0.0218	0.0254	0.1156	0.1182	0.2527	0.2526
7(84Ti2Sn2Zr5Al4Mo3Cr)	0.0187	0.0235	0.1185	0.2051	0.2091	0.2091

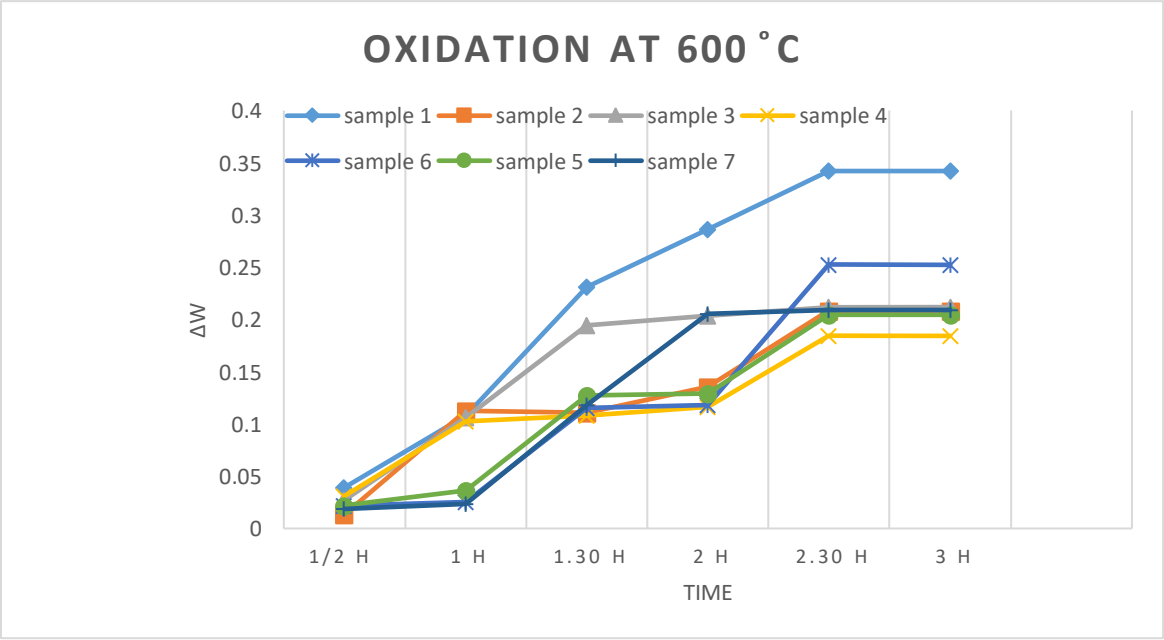


Figure 6. Oxidation at 600°C for all samples

Table 6. Oxidation at 700°C

sample	ΔW After 30 min	ΔW After 1 h	ΔW After 1.30 h	ΔW After 2h	ΔW After 2:30h	ΔW After 3h
1(83Ti2Sn2Zr5Al4Mo4Cr)	0.0507	0.0585	0.4067	0.6501	1.2360	1.2361
2(82Ti2Sn2Zr6Al4Mo4Cr)	0.2116	0.2984	0.2804	0.2986	0.3626	0.3624
3(84Ti2Sn2Zr4Al4Mo4Cr)	0.3057	0.316	0.3160	0.3372	0.7821	0.7822
4(82Ti2Sn2Zr5Al5Mo4Cr)	0.0110	0.1270	0.1650	0.2091	0.2381	0.2381
5(84Ti2Sn2Zr5Al3Mo4Cr)	0.1020	0.1230	0.1621	0.2122	0.2324	0.2324
6(82Ti2Sn2Zr5Al4Mo5Cr)	0.2458	0.2649	0.2933	0.4377	0.2933	0.2932
7(84Ti2Sn2Zr5Al4Mo3Cr)	0.2020	0.2150	0.2812	0.5681	0.6167	0.6167

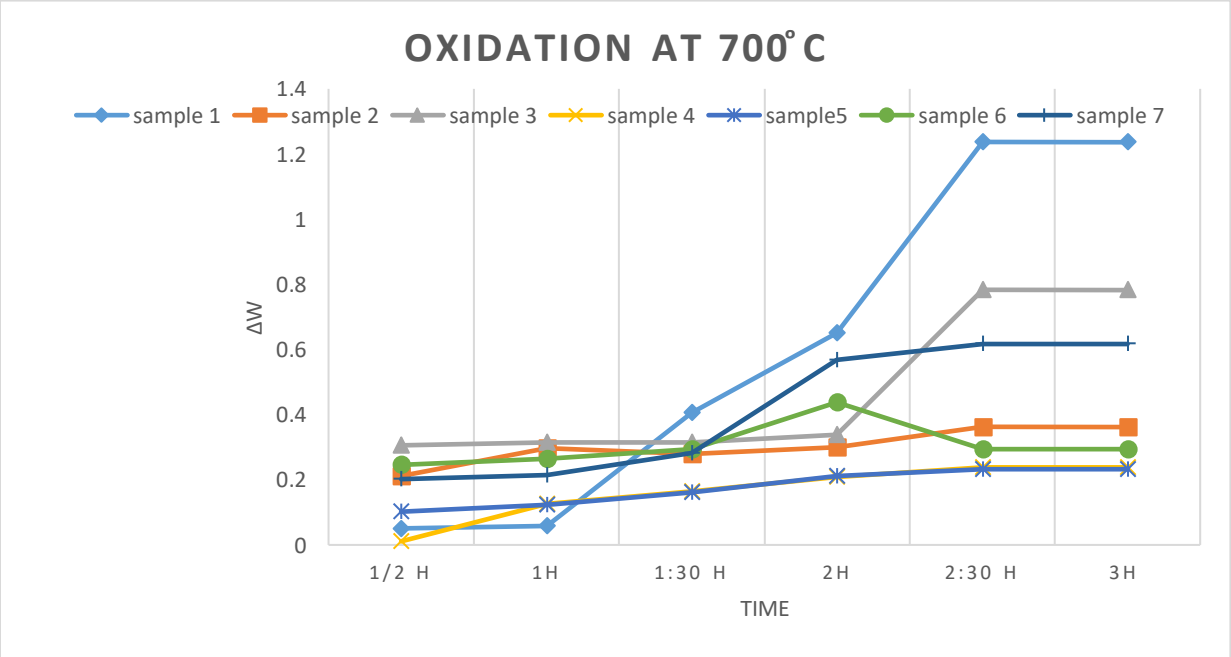


Figure 7. Oxidation at 700°C for all samples

Table 7. Oxidation at 800°C

sample	ΔW After 30 min	ΔW After 1 h	ΔW After 1.30 h	ΔW After 2h	ΔW After 2:30h	ΔW After 3h
1(83ti2sn2zr5al4mo4cr)	0.3200	0.3781	0.401	0.4386	0.6081	0.6082
2(82ti2sn2zr6al4mo4cr)	0.6372	0.5842	0.7914	0.7983	1.3201	1.3200
3(84ti2sn2zr4al4mo4cr)	0.0078	0.1216	0.2318	0.4160	0.4832	0.4833
4(82ti2sn2zr5al5mo4cr)	0.0921	0.1014	0.1098	0.1532	0.1834	0.1833
5(84ti2sn2zr5al3mo4cr)	0.0880	0.1798	0.2031	0.2487	0.4012	0.4013
6(82ti2sn2zr5al4mo5cr)	0.3623	0.4027	0.4302	0.4732	0.5094	0.5094
7(84ti2sn2zr5al4mo3cr)	0.1270	0.3935	0.4929	0.5063	0.5154	0.5154

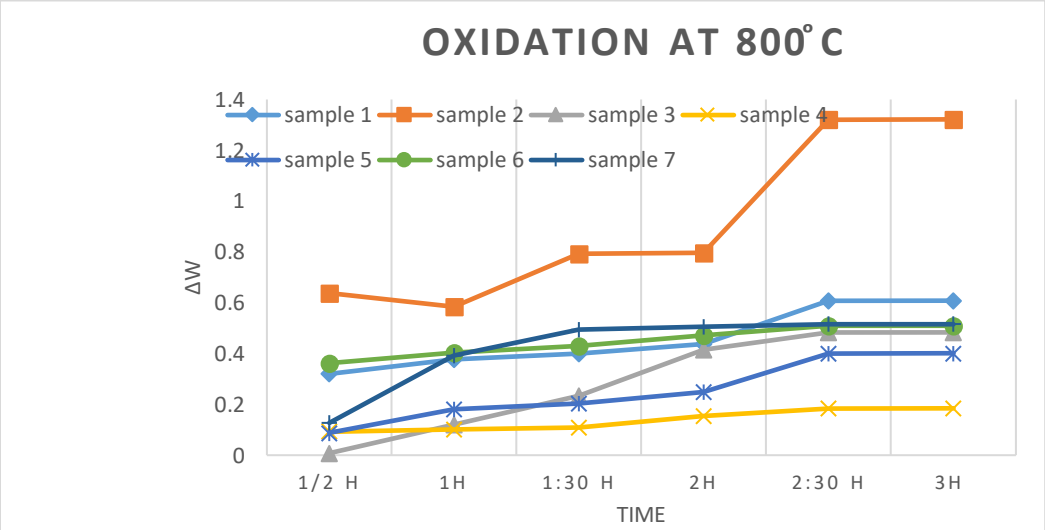


Figure 8. Oxidation at 800°C for all samples

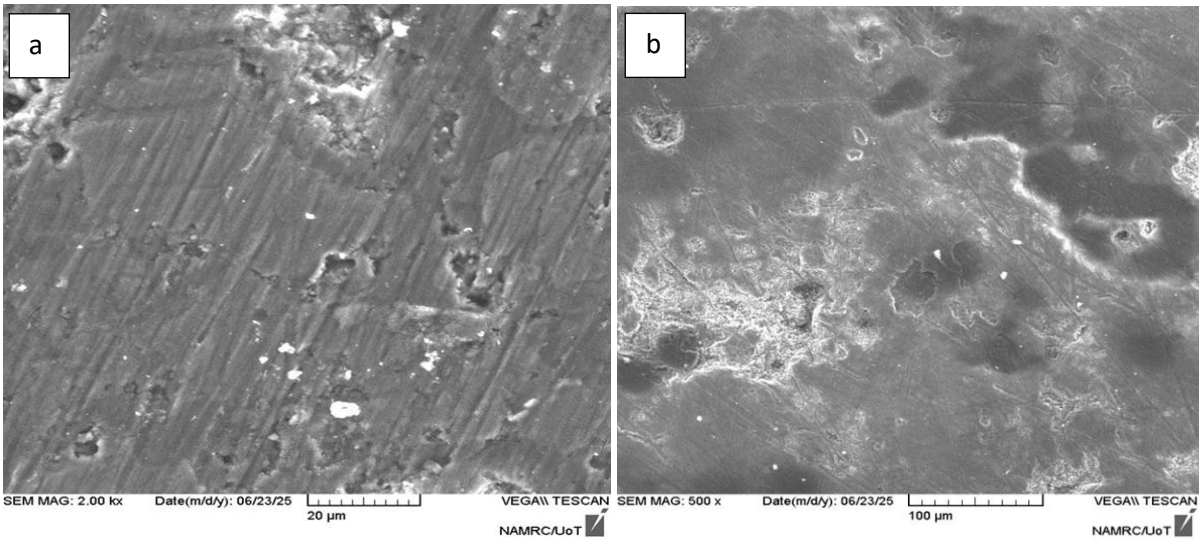


Figure 9. SEM of alloy 4 after oxidation at a) 600 °C; b) 700°C.

Thermal shock

The sample was heated to 600°C and then quenched in air or water. This generates rapid variations in volume inside the material. This may induce internal thermal stresses that can cause cracking or damage to the oxide layer or the material itself. Ti-17 has rather excellent resistance to thermal shock at 600°C as illustrated in Figs. 10-12; Table 8 and 9. Surface cracking or flaking may occur but they seldom result in any interior structural degradation. Some surface damage may occur, but it will not lead to immediate structural failure. The alloy is relatively suitable for use in applications subject to moderate cyclic temperature changes. In 700°C It continues to form but becomes more brittle. It becomes inflexible under expansion; Pure titanium has relatively good resistance to thermal shock due to its low coefficient of thermal expansion. The presence of aluminum increases the stability of the surface layer and reduces cracking in the oxide layer. Chromium is one of the most important elements, as it forms a flexible and cohesive oxide layer that reduces cracking of the oxides when the metal expands and contracts (Donachie, 2000; Leyens & Peters, 2006). Zirconium improves the bond between the surface layer and the metal for all this alloy No. 4 with composition (82Ti2Sn2Zr5Al5Mo4Cr) is the best alloy at all temperatures

Table 8. Thermal shock at 600°C

sample	ΔW After 30 min	ΔW After 1 h	ΔW After 1.30 h	ΔW After 2 h	ΔW After 2.30 h	ΔW After 3 h
1(83ti2sn2zr5al4mo4cr)	0.0392	0.1083	0.2310	0.2861	0.3421	0.3421
2(82ti2sn2zr6al4mo4cr)	0.0134	0.1130	0.1106	0.1354	0.2086	0.2086
3(84ti2sn2zr4al4mo4cr)	0.0271	0.1065	0.1941	0.2035	0.2117	0.2116
4(82ti2sn2zr5al5mo4cr)	0.0311	0.1021	0.1083	0.1161	0.1845	0.1844
5(84ti2sn2zr5al3mo4cr)	0.0221	0.0368	0.1270	0.1289	0.2045	0.2045
6(82ti2sn2zr5al4mo5cr)	0.0218	0.0254	0.1156	0.1182	0.2527	0.2526
7(84ti2sn2zr5al4mo3cr)	0.0187	0.0235	0.1185	0.2051	0.2091	0.2091

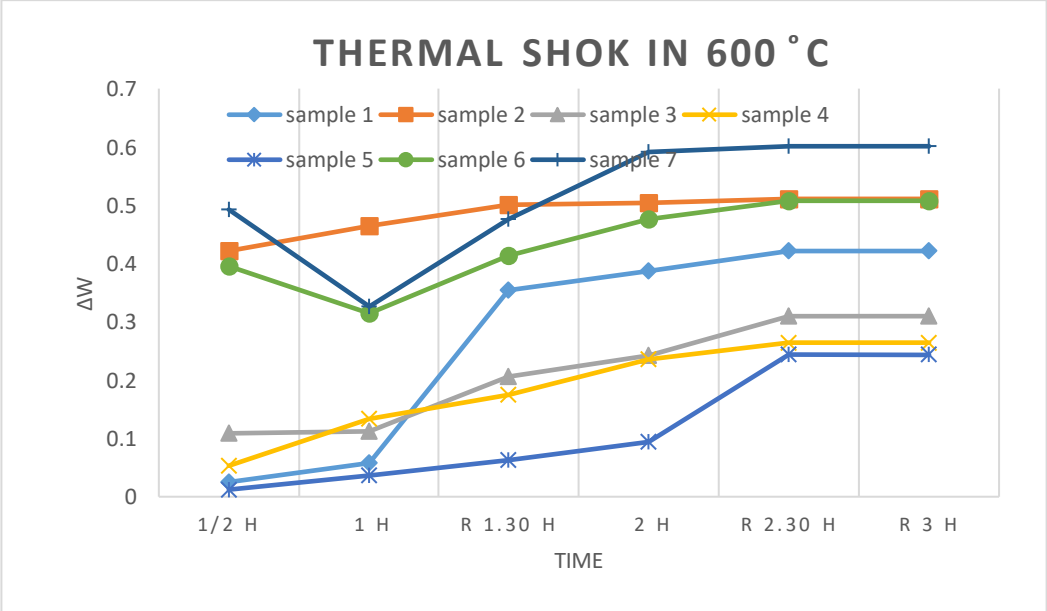


Figure 10. Thermal shock at 600°C for all samples

Table 9. Thermal shock at 700°C

sample	ΔW After 30 min	ΔW After 1 h	ΔW After 1.30 h	ΔW After 2h	ΔW After 2:30h	ΔW After 3h
1(83ti2sn2zr5al4mo4cr)	0.0507	0.0585	0.4067	0.6501	1.2360	1.2361
2(82ti2sn2zr6al4mo4cr)	0.2116	0.2984	0.2804	0.2986	0.3626	0.3624
3(84ti2sn2zr4al4mo4cr)	0.3057	0.316	0.3160	0.3372	0.7821	0.7822
4(82ti2sn2zr5al5mo4cr)	0.0110	0.1270	0.1650	0.2091	0.2381	0.2381

5(84ti2sn2zr5al3mo4cr)	0.1020	0.1230	0.1621	0.2122	0.2324	0.2324
6(82ti2sn2zr5al4mo5cr)	0.2458	0.2649	0.2933	0.4377	0.2933	0.2932
7(84ti2sn2zr5al4mo3cr)	0.2020	0.2150	0.2812	0.5681	0.6167	0.6167

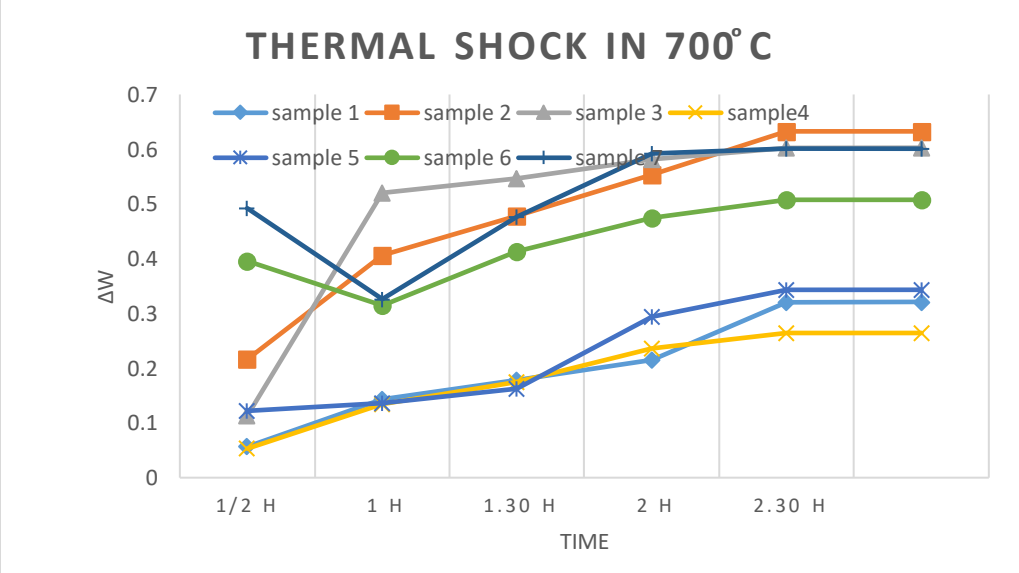


Figure 11. Thermal shock at 700°C for all samples

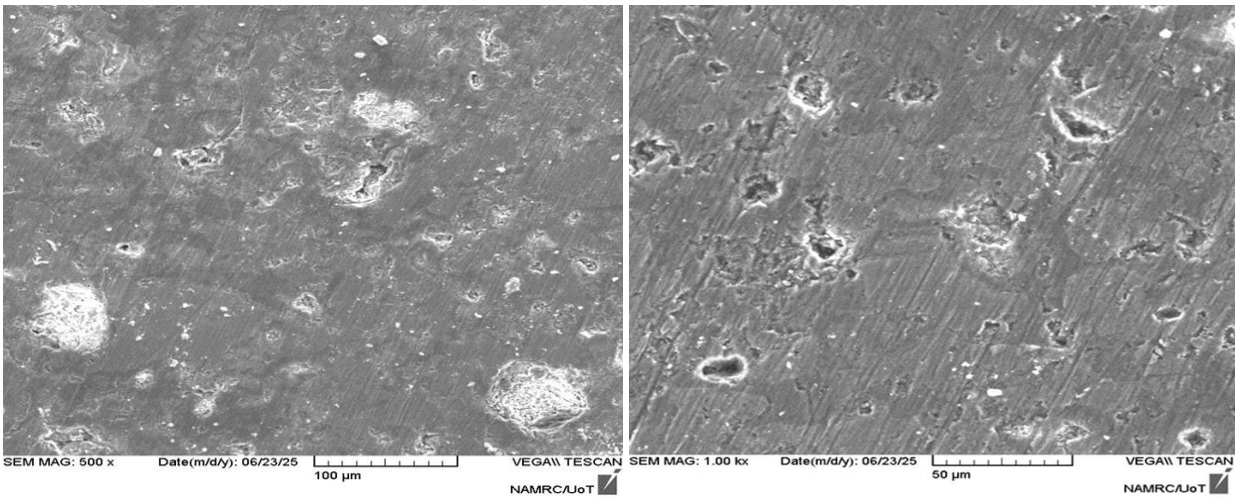


Figure 12. SEM of alloy 4 after thermal shock at: a) 600°C; b) 700°C.

4. CONCLUSION

In the current work, the effect of compositional variations on the microstructure, hardness, oxidation resistance and thermal shock behavior of seven powder metallurgy Ti-17 alloy compositions was comprehensively examined. The following conclusions may be taken from the experimental results:

- XRD, optical microscopy and SEM/EDX investigations verified the effective production of dense Ti-17 alloys with the distinctive dual-phase α+β microstructure by powder metallurgy processing. The absence of unwanted secondary phases indicated that homogeneity of alloy during sintering was successful.
- The phase distribution and microstructural refinement are sensitive to the balance between α-stabilizing elements (Al and Sn) and β-stabilizing elements (Mo and Cr). The most homogenous and refined alpha+beta microstructure was seen in Alloy No. 4 (82Ti-2Sn-2Zr-5Al-5Mo-4Cr) which demonstrated the best combination of mechanical and thermal characteristics.

- The Brinell hardness of the manufactured alloys was in the range of 385–402 HB, while the reference Ti-17 alloy was 396 HB. The maximum hardness was obtained for alloy No. 4 which amounted to 402 HB, which is an actual improvement of around 1.52 % compared to the reference alloy. The increase in hardness is attributable to the synergic effects of β-phase stability, solid-solution strengthening and microstructural refinement, caused by the optimum contents of Mo and Al.
- As the temperature increased, the resistance to oxidation at high-temperature reduced because the formation of oxide and diffusion of oxygen were accelerated. Alloy No. 4 displayed the lowest oxidation weight increase at 600, 700 and 800°C, indicating the best oxidation resistance among the compositions examined. This behavior was explained by the creation of a thick and adherent protective oxide layer with refined microstructure and decreased porosity which inhibited the oxygen entry into the alloy matrix.
- The cyclic thermal loading resistance was significantly increased by the composition improvement as seen in the thermal shock tests. Alloy No. 4 exhibited better performance because of the stable α+β phase balance and better oxide-scale adherence, which decreased the tendency of oxide cracking and spallation during repeated heating and cooling cycles. However, the thermal shock data sets should be cross-checked since the present article has repeated values in the respective tables.
- The findings obtained overall showed that the optimization of chemical composition of Ti-17 alloys by powder metallurgy is an efficient way to improve the hardness, oxidation resistance and thermal shock performance concurrently. The optimized alloy composition 82Ti–2Sn–2Zr–5Al–5Mo–4Cr is especially promising for high-temperature aerospace applications such as compressor discs, turbine components and other engineering applications which require high mechanical strength coupled with excellent oxidation resistance and cyclic thermal loading.

Acknowledgement
We thank University of Babylon and laboratory staffs who help me to complete the experimental work.

Author Contributions
Eman S. Obaid: was conducted the experimental work and write the draft manuscript; Ekbal Mohammed Saeed Salih and Saad Hameed Al-Shafaie conducted the discussion of the results and revised manuscript final draft.

Ethical issues
Not applicable. This study does not involve any experiments on humans or animals. Hence, ethical approval was not required.

Informed consent
Not applicable.

Funding
This research did not receive any external funding like specific grant from funding agencies in the public, commercial, or nonprofit sectors.

Conflict of Interest
The authors declare that they have no conflicts of interest, competing financial interests or personal relationships that could have influenced the work reported in this paper.

Data and materials availability
All data associated with this study will be available based on the reasonable request to corresponding author.

REFERENCES

1. Abd-Elaziem W, Darwish MA, Hamada A, Daoush WM. Titanium-based alloys and composites for orthopedic implants applications: a comprehensive review. Mater Des 2024; 241:112850. doi:10.1016/j.matdes.2024.112850
2. Abed KM, Radhi NS, Jasim AH, Al-Khafaji ZS, Radhi S, Hussien SA. Study the effect of adding zirconia particles to nickel-phosphorus electroless coatings as product innovation on stainless steel substrate. Open Eng 2022; 12(1):1038–1045.

doi:10.1515/eng-2022-0364
3. Ali LH, Hassan RF, Hussein HH. Experimental and analytical investigations of torsional strength in ultra-high-performance concrete beams with transverse openings. Buildings 2024; 14(8):2315. doi:10.3390/buildings14082315
4. Antunes RA, Salvador CAF, Oliveira MCL. Materials selection of optimized titanium alloys for aircraft applications. Mater Res 2018; 21:e20170979. doi:10.1590/1980-5373-mr-2017-0979
5. Besisa NHA, Yajima T. Titanium-based alloys: classification and diverse applications. In: Titanium-Based Alloys—Characteristics and Applications. IntechOpen; 2024. doi:10.5772/intechopen.1005269
6. Court SA, Gatenby KM, Lloyd DJ. Factors affecting the strength and formability of alloys based on Al-3 wt.% Mg. Mater Sci Eng A 2001; 319:443–447. doi:10.1016/S0921-5093(00)02018-9
7. Donachie MJ. Titanium: A Technical Guide. 2nd ed. Materials Park, OH: ASM International; 2000. doi:10.31399/asm.tb.ttg2.9781627082693
8. Elshaer RN, Ibrahim KM. Applications of titanium alloys in aerospace manufacturing: a brief review. Bull Tabbin Inst Metall Stud 2022; 111(1):60–69. doi:10.21608/tims.2023.174504.1007
9. Gao K, Zhang Y, Yi J, Dong F, Chen P. Overview of surface modification techniques for titanium alloys in modern material science: a comprehensive analysis. Coatings 2024; 14(1):148. doi:10.3390/coatings14010148
10. Jasim AH, Radhi NS. Review on improvement the turbine oxidation and hot resistant against corrosion by nickel-based superalloy. Mater Mech Eng Technol 2024; 2024(4):89–104. doi:10.52209/2706-977X
11. Jawed SF, Rabadia CD, Khan MA, Khan SJ. Effect of alloying elements on the compressive mechanical properties of biomedical titanium alloys: a systematic review. ACS Omega 2022; 7(34):29526–29542. doi:10.1021/acsomega.2c02096
12. Leyens C, Peters M. Titanium and Titanium Alloys: Fundamentals and Applications. Weinheim: Wiley-VCH; 2006.
13. Luo J, Li L, Li MQ. The flow behavior and processing maps during the isothermal compression of Ti-17 alloy. Mater Sci Eng A 2014; 606:165–174. doi:10.1016/j.msea.2014.03.103
14. Marin E, Lanzutti A. Biomedical applications of titanium alloys: a comprehensive review. Materials 2023; 17(1):114. doi:10.3390/ma17010114
15. Moshier MA, Nicholas T, Hillberry BM. Load history effects on fatigue crack growth threshold for Ti-6Al-4V and Ti-17 titanium alloys. Int J Fatigue 2001; 23(3):253–258.
16. Narayan RJ. Materials for Medical Devices. Materials Park, OH: ASM Int 2012. doi:10.31399/asm.hb.v23.9781627081986
17. Niinomi M. Recent research and development in titanium alloys for biomedical applications and healthcare goods. Sci Technol Adv Mater 2003; 4(5):445–454. doi:10.1016/j.stam.2003.09.002
18. Quinn J, McFadden R, Chan CW, Carson L. Titanium for orthopedic applications: an overview of surface modification to improve biocompatibility and prevent bacterial biofilm formation. iScience 2020; 23(11):101745. doi:10.1016/j.isci.2020.101745
19. Radhi NS, Al-Khafaji Z. Investigation biomedical corrosion of implant alloys in physiological environment. Int J Mech Prod Eng Res Dev 2018; 8(4). doi:10.24247/ijmperdaug201827
20. Shi X, Zeng WD, Shi CL, Wang QS, Jia ZQ, Wang M. Effect of microstructure on fracture toughness and fatigue crack growth behavior of Ti-17 alloy. Metals 2016; 6(8):186. doi:10.3390/met6080186
21. Tao S, Zhi G, Zhang Z, Liu Y, Li H, Xie S, Xie P, Chen H. Effect of multi-stage heat treatment on the microstructure and mechanical properties of Ti-6Al-4V alloy deposited by high-power laser melting deposition. Mater Sci Eng A 2024; 895:146226. doi:10.1016/j.msea.2024.146226
22. Tarín P, Fernández AL, Simón AG, Badía JM, Piris NM. Transformations in the Ti-5Al-2Sn-2Zr-4Mo-4Cr (Ti-17) alloy and mechanical and microstructural characteristics. Mater Sci Eng A 2006; 438–440:364–368.
23. Teixeira JDC, Appolaire B, Aeby-Gautier E, Denis S, Cailletaud G, Späth N. Transformation kinetics and microstructures of Ti-17 titanium alloy during continuous cooling. Mater Sci Eng A 2007; 448(1–2):135–145.
24. Valdez B, Schorr M, Zlatev R, Carrillo M, Stoytcheva M, Alvarez L, Eliezer A, Rosas N. Corrosion control in industry. In: Environmental and Industrial Corrosion—Practical and Theoretical Aspects. IntechOpen 2012. doi:10.5772/51987
25. Wang T, Guo HZ, Tan LJ, Yao ZK, Zhao Y, Liu PH. Beta grain growth behaviour of TG6 and Ti-17 titanium alloys. Mater Sci Eng A 2011; 528(21):6375–6380.
26. Xu JW, Zeng WD, Zhao YW, Jia ZQ, Sun X. Effect of globularization behavior of the lamellar alpha on tensile properties of Ti-17 alloy. J Alloys Compd 2016; 673:86–92.